HHS Public Access

Author manuscript

Annu Rev Anal Chem (Palo Alto Calif). Author manuscript; available in PMC 2016 June 16.

Published in final edited form as:

Annu Rev Anal Chem (Palo Alto Calif). 2016 June 12; 9(1): 95–115. doi:10.1146/annurev-anchem-071015-041514.

Advances in Magnetic Resonance Imaging Contrast Agents for Biomarker Detection

Sanhita Sinharay[1] and **Mark D. Pagel**[1,2]

Sanhita Sinharay: sinharay@email.arizona.edu; Mark D. Pagel: mpagel@email.arizona.edu

[1]Department of Chemistry and Biochemistry, University of Arizona, Tucson, Arizona 85724

[2]Department of Medical Imaging, University of Arizona, Tucson, Arizona 85724

Abstract

Recent advances in magnetic resonance imaging (MRI) contrast agents have provided new capabilities for biomarker detection through molecular imaging. MRI contrast agents based on the T_2 exchange mechanism have more recently expanded the armamentarium of agents for molecular imaging. Compared with T_1 and T_2^* agents, T_2 exchange agents have a slower chemical exchange rate, which improves the ability to design these MRI contrast agents with greater specificity for detecting the intended biomarker. MRI contrast agents that are detected through chemical exchange saturation transfer (CEST) have even slower chemical exchange rates. Another emerging class of MRI contrast agents uses hyperpolarized ^{13}C to detect the agent with outstanding sensitivity. These hyperpolarized ^{13}C agents can be used to track metabolism and monitor characteristics of the tissue microenvironment. Together, these various MRI contrast agents provide excellent opportunities to develop molecular imaging for biomarker detection.

Keywords

MRI contrast agents; T_1; T_2^*; T_2 exchange; chemical exchange saturation transfer; hyperpolarized ^{13}C

1. INTRODUCTION

The imaging of molecular biomarkers has great potential to complement anatomical imaging by interrogating pathological tissues at an early disease state and to assess the early response to treatment (1). A variety of magnetic resonance imaging (MRI) contrast agents have been developed to improve the molecular imaging of many disease types. However, MRI suffers from inherently low detection sensitivity that requires ~10 μM to ~10 mM of a contrast agent, depending on the MRI contrast mechanism described below (2–5). Therefore, MRI contrast agents can be designed only for targeting biomarkers that are present at high ~10 μM to ~10 mM concentrations in vivo. Furthermore, compelling evidence exists that metallic exogenous contrast agents that are delivered into cells at ~10 μM to ~10 mM can

DISCLOSURE STATEMENT

The authors are not aware of any affiliations, memberships, funding, or financial holdings that might be perceived as affecting the objectivity of this review.

alter the behavior of the cells and can also cause cell death (6, 7). For these reasons, most MRI contrast agents for molecular imaging have had the greatest impact in detecting extracellular molecular biomarkers (as an exception, hyperpolarized ^{13}C MRI contrast agents are nonmetallic and can interrogate intracellular metabolism).

Many types of biomarkers can be identified with MRI contrast agents. Biomarkers have traditionally been considered to be atomic or molecular targets, such as abundant proteins in the extracellular matrix, ions, and metabolites. We consider these types of extracellular biomarkers to be target limited because the 1:1 interaction between the agent and target is primarily limited by the concentration of the molecular target (8, 9). Alternatively, environmental biomarkers can also inform radiologists about disease, such as the status of extracellular hypoxia, acidosis, redox potential, and temperature. Because these conditions are ubiquitous throughout the extracellular tissue environment (at least at a spatial scale larger than a single imaging voxel) and affect each agent in the tissue environment, we refer to these biomarkers as agent limited because their detection is limited by the concentration of the agent in the environment. As another example, a low concentration of enzyme that efficiently catalyzes changes to a contrast agent can often process a high concentration of agent for adequately sensitive detection. Therefore, enzyme activity can also be considered to be a biomarker of an active extracellular tissue environment (10).

On a nano- to micrometer scale, MRI contrast agents have been packaged in macromolecular vehicles such as cells, liposomes, and nanoparticles (11–14). These contrast agents can be used to track the pharmacokinetic transport of these macromolecular systems for applications that range from nanoparticle drug delivery to cell tracking. These agents can also interrogate physiological tissue properties related to pharmacokinetic transport, such as vascular permeability and perfusion, and the integrity of the blood-brain barrier (15, 16). Therefore, these MRI contrast agents are used as pharmacokinetic agents to differentiate normal tissue from pathological tissue during preclinical and clinical imaging studies.

This review focuses on the four major classes of MRI contrast agents. The class of relaxation-based T_1 and T_2 MRI contrast agents has matured during the past 30 years. The subclass of T_2 exchange (T_{2ex}) contrast agents has been rediscovered during the past few years and has the potential to bring great innovation to this field. In addition, the fields of exogenous chemical exchange saturation transfer (CEST) MRI contrast agents and hyperpolarized ^{13}C MRI contrast agents have rapidly developed during the past decade.

2. T_1 AND T_2^* MRI CONTRAST AGENTS

A variety of MRI acquisition protocols can generate image contrast based on different T_1 or T_2^* relaxation time constants of normal and pathological tissues (17). Exogenous T_1 and T_2^* contrast agents in pathological tissues that accumulate to different extents in normal and pathological tissues can greatly improve the image contrast between these tissues, allowing the pathological tissue to be more easily recognized in the image (Figures 1 and 2*d*) (18, 19).

2.1. T_1 AND T_2^* Relaxation Mechanisms

The first exogenous contrast agents for MRI studies were used to accelerate the rate that excited magnetic resonance (MR) states “relax” to equilibrium. This rate is often represented by the T_1 relaxation time constant, so that these contrast agents are known as T_1 agents. These agents often use gadolinium or manganese that have unpaired electrons, which can rapidly relax the excited MR signal of water (20, 21). Macrocyclic chelates or other molecules that surround the metal ion can be designed to interact with a biomarker in ways that modulate the distance between the metal and water or the rate of interaction between the metal and water, both of which affect T_1 relaxation (8, 9). A T_1-weighted MRI protocol can then monitor changes in T_1 relaxation, which is used to indirectly detect the biomarker.

A population of protons on water molecules must have the same MR frequency (also known as the chemical shift) with the same phase for adequate detection of the net water MR signal. Importantly, the MR frequencies of individual water protons can change, which causes the MR frequencies to become incoherent, resulting in a loss of detectable net MRI signal from the water. Paramagnetic MRI contrast agents, such as iron oxide nanoparticles, can create small local magnetic fields as large as a 20-μm scale that are randomly oriented relative to the main magnetic field of the MRI instrument (22). These local magnetic fields cause the MR frequencies of individual water protons to accelerate or decelerate, causing incoherence of the MR frequencies of these protons. This rate of signal reduction is often represented by the T_2^* relaxation time constant, so that these contrast agents are known as T_2^* agents. These agents can be designed to interact with a biomarker in ways that can change the tumbling rate of the agent, whereby a slower tumbling rate prolongs differences in local magnetic fields and accelerates T_2^* relaxation (8, 9). Agents can also be designed to form superparamagnetic clusters that increase differences in local magnetic fields and accelerate T_2^* relaxation of the sample. A T_2-weighted MRI protocol can then monitor changes in T_2^* relaxation, which is used to indirectly detect the biomarker.

2.2. Pharmacokinetic Relaxation-Based Agents

The development of new T_1 and T_2^* MRI contrast agents continues to be proliferative, with an average of approximately 60 new agents reported each year for the past decade. Therefore, recent progress with these agents is described in general terms rather than by providing specific examples. As a trend, a tremendous number of nanoparticles have been developed with MRI contrast agents (23). These developments address the inherent insensitivity of T_1 and T_2^* MRI contrast agents by containing many MRI agents within the nanoparticle, which reduces concerns about this agent-limited approach. Also, the tumbling time of the nanoparticle is often much slower than the small-molecule MRI contrast agent, which enhances the relaxation properties of each agent. Together, these two effects can increase the T_1 or T_2^* relaxation effects by one to three orders of magnitude (depending on the size of the nanoparticle). However, the pharmacokinetic accumulation of nanoparticles in tissues can often be slow, which often complicates in vivo MRI studies. More importantly, the pharmacokinetic washout rates of nanoparticle agents are slow, often taking more than 24 h for adequate clearance. This raises major concerns regarding toxicity, especially for agents that contain Gd^{3+} or Mn^{2+} ions, or iron-based particles other than iron oxides, each of which has shown longer-term toxic effects (24, 25). Furthermore, the current contrast agents

that are approved by the Food and Drug Administration for pharmacokinetics studies already satisfy clinical needs, which provides little motivation to invest efforts to create new T_1 MRI contrast agents for pharmacokinetics studies. Currently, T_2^* contrast agents are not marketed in the United States because of insufficient clinical demand, which also severely reduces motivation to develop new T_2^* contrast agents for pharmacokinetics-based diagnoses. As an exception, T_2^* MRI contrast agents that can track the pharmacokinetics of nanoparticle drug delivery systems continue to be a subject of active research (26).

A remarkable recent development consists of T_2^* contrast agents that can detect cell receptors in vivo. First developed in the late 1990s, these agents were assumed to have insufficient detection sensitivity for this target-limited approach, owing to the subnanomolar concentration range of receptors on cell surfaces, even for highly overexpressed cell receptors, whereas T_1 and T_2^* contrast agents require ~100- and ~10-μM concentrations for minimum detection (27, 28). However, recent in vivo studies have shown that tumor tissues that highly express the HER-2 receptor can be targeted with an anti-HER-2 antibody that is labeled with iron oxide (Figure 2) (29, 30). In this case, the HER-2 receptor can internalize the antibody into the cell and quickly recycle to the cell surface to internalize additional labeled antibodies in a time frame that is reasonable for in vivo MRI studies. Even though the agent is internalized into cells, the detection of the cell receptor occurs in the extracellular environment. Additional research is required to interrogate the cell internalization and receptor recycling mechanisms to better understand which cell receptors may be detected using targeting nanoparticles that are labeled with T_2^* contrast agents.

As another general trend during the past few years, multimodal agents have been synthesized and characterized that can be detected with MRI and positron emission tomography or with MRI and optical imaging (31, 32). However, the large differences in detection sensitivities between contrast agents for MRI and these other imaging modalities must be considered to make a practical agent for multimodal imaging (33). In addition, the results from MRI and the other imaging modalities should be complementary rather than redundant to provide more diagnostic information, such as imaging results that report on pharmacokinetic properties at different spatial or longitudinal scales (34). This complementary information from MRI will likely be limited to the extracellular environment, for reasons discussed above. Until these hurdles can be addressed, the field of multimodality contrast agents that include MRI may struggle to find practical clinical utility.

2.3. Responsive Relaxation-Based Agents

Biomarker-responsive T_1 and T_2^* agents that have been developed during the past few years have primarily focused on the detection of molecular conditions of the tissue environment. This focus is driven by the poor detection sensitivity of MRI, often requiring an abundance of the biomarker for detection, and there is no greater abundance than the entire environment of the tissue or tissue compartments. For example, an acidic tissue compartment or a reducing environment can cause an agent to become more protonated, which can alter the water accessibility to the metallic component of the agent that causes a change in T_1 relaxation time (35). As another example, a Gd(III) chelate that binds to zinc can then tightly bind to human serum albumin, which causes a slower tumbling time for the Gd(III) chelate

that enhances T_1 relaxation (Figure 3) (36). Unfortunately, most of these agents have not been tested in vivo, because accounting for the concentration of the agent within in vivo tissues is a major complication that has impeded translational studies.

3. T_{2ex} CONTRAST AGENTS

This unique process of T_2 exchange relaxation (also known as T_{2ex}) has been exploited in nuclear magnetic resonance (NMR) spectroscopy for more than 45 years to reduce the NMR signal from the solvent during studies of dilute samples (37, 38). T_{2ex} agents were first employed for MRI studies in 1988, but they have only recently been rediscovered for in vivo MRI studies (39, 40). This lag in developing T_{2ex} agents is partly due to the relative insensitivity of these agents compared with the other relaxation-based agents. This lower sensitivity is caused by a slower 10^4–10^7-Hz chemical exchange rate of protons between the T_{2ex} agent and water, relative to 10^7–10^9-Hz exchange rates of water molecules between bulk water and the solvation shells of T_1 and T_2^* agents (41). Yet this slower rate provides more opportunities to develop contrast agents that can respond to biomarkers by changing their proton exchange rates, which may improve specificity for detecting the intended biomarker. Therefore, there is a rapidly developing interest in T_{2ex} MRI contrast agents to improve the specificity for biomarker detection.

3.1. The T_{2ex} Mechanism

As described in Section 2.1, T_2 relaxation of the water MR signal depends on the rate at which water protons have MR frequencies that accelerate or decelerate relative to each other, causing the net MR signal to become incoherent. A water proton can accelerate or decelerate in MR frequency when it exchanges with a proton on a contrast agent. Moderately rapid chemical exchange at 10^4–10^7 Hz can create sufficient changes in MR frequencies of a sufficient population of water protons to cause detectable T_{2ex} relaxation. Importantly, the incoherence of the net MR signal from the labile protons is accentuated when the MR frequency of the agent is very different from the MR frequency of water.

Although T_2-weighted MRI can detect changes in T_{2ex} relaxation, the T_2 relaxation time constant of the sample is more often used to quantify T_{2ex}. This improves the detection of small changes in T_2 relaxation caused by the T_{2ex} effect and may also be used to better characterize the physiochemical properties of the T_{2ex} agent. Multi-echo MRI pulse sequences can often be employed to accurately measure T_2 relaxation time constants, which do not require additional scan time relative to single-echo, T_2-weighted MRI protocols in most cases. Therefore, the measurement of T_2 relaxation time constants for assessing T_{2ex} agents can easily be translated to clinical radiology practice.

3.2. Pharmacokinetic T_{2ex} Agents

Paramagnetic MRI contrast agents can cause proximal protons to have a large pseudocontact shift, producing a very large MR frequency for the proton (42). This large MR frequency can generate a large T_{2ex} relaxation effect. For example, a derivative of a Eu(III)-DOTA macrocyclic chelate has an MR frequency of 42.5 ppm that can cause remarkable darkening of the MR image when the agent is administered at a moderate 0.25 mmol kg^{-1} (Figure 4)

(40). This characteristic of the Eu(III)-DOTA agent was used to track the pharmacokinetics of the agent in kidney tissue during a preclinical in vivo study. A series of Dy(III)-DOTA derivatives with similar MR frequencies but with different chemical exchange rates were also tested, showing that the chemical exchange rate must be tuned to an ideal value relative to the MR frequency to produce the greatest T_{2ex} effect (43). Because an MR frequency depends on the magnetic field strength of the MRI instrument, different Dy(III)-DOTA derivatives with ideal T_{2ex} relaxation effects can be matched to the MRI instrument. This example shows the merits of using a multidisciplinary approach that combines chemistry and physics of MRI to produce a synergistic biomedical diagnostic system.

Although diamagnetic contrast agents do not possess a large MR frequency relative to water, two examples have shown a T_{2ex} effect that can be employed for in vivo MRI studies. Iopamidol (Isovue™, Bracco Diagnostics Inc.) is an iodinated contrast agent that is clinically approved for computed tomography (CT) studies (39). Glucose is clinically approved for IV administration to treat carbohydrate and fluid depletion (44). Both of these agents have hydroxyl groups that have moderately fast chemical exchange rates that are well tuned to generate a T_{2ex} effect at clinical and preclinical MRI magnetic field strengths. However, the MR frequencies of these hydroxyl groups are a low ~1 to ~3 ppm relative to the MR frequency of water, which reduces their T_{2ex} effect on a per molecule basis. Fortunately, these agents are highly biocompatible and are clinically approved for IV injection at 976 mM for iopamidol and up to 20 mM for glucose, so that this agent-limited approach is not a limitation in practice. This high concentration can then generate significant T_{2ex} relaxation. These two examples show that other clinically approved CT contrast agents and sugars can also be used as T_{2ex} agents, providing many new opportunities to develop and test agents that have a good pathway to clinical translation. The pharmacokinetics of CT agents can be tracked to study angiography and tissue perfusion, whereas the pharmacokinetics of glucose may be used to assess vascular permeability that is a hallmark of angiogenic tumors. These major biomedical diagnostic applications further strengthen the case for further developing these two classes of diamagnetic T_{2ex} agents.

3.3. Responsive T_{2ex} Agents

Because the field of T_{2ex} contrast agents for MRI is relatively new, the development of responsive T_{2ex} agents has only one current example (45). A derivative of a Tm(III)-DOTA macrocyclic chelate has a slow chemical exchange rate of 4,700–14,500 Hz that cannot generate a significant T_{2ex} relaxation effect, despite the large 19-, −29-, and −49-ppm MR frequencies of the exchangeable protons on the agent. However, after reacting with the oxidative by-products of nitric oxide, the agent has a chemical exchange rate exceeding 140,000 Hz. Importantly, the T_1 relaxation properties of the agent do not change before and after treatment with nitric oxide, which confirms that the Tm(III) macrocyclic chelate is a T_{2ex} agent rather than changing dipolar T_2 relaxation properties (which would also change T_1 relaxation). The invariant T_1 relaxation properties can be used as a control MR signal to account for the concentration of the agent, which greatly improves quantification during the biomarker study. More specifically, the T_2/T_1 ratio of relaxation time constants is concentration independent, but this ratio increases after the agent is treated with nitric oxide. Therefore, monitoring this ratio with MRI can be used to noninvasively detect extracellular

nitric oxide, which is a useful biomarker of tumor angiogenesis and apoptosis. Although this agent uses a target-limited approach, a sufficient amount of nitric oxide can be produced by pathological tissues for sufficient detection of the responsive T_{2ex} agent. Also, this agent detects nitric oxide that would be available only in the extracellular environment, because the polar agent is cell impermeable.

4. CEST MRI CONTRAST AGENTS

CEST MRI contrast agents have the slowest chemical exchange rates relative to T_1, T_2, and T_{2ex} contrast agents (41). As a result, these agents have the least-sensitive detection, requiring a minimum concentration in the single-millimolar range. Yet as an advantage, this slow exchange rate provides opportunities to design agents with specific exchange rates or specific changes in exchange rates, which provides outstanding diagnostic selectivity. For these reasons, CEST agents are rarely used for anatomical imaging and are most commonly designed to be responsive to specific extracellular biomarkers. In addition, applications of pharmacokinetic CEST agents are also emerging.

CEST MRI has also been developed to detect endogenous biomolecules that exchange protons with water. Examples include the detection of endogenous glutamate, creatine, and glycosaminoglycans (46–48). As another example, the general pool of tissue proteins has amide and amine groups that exchange protons with water at rates that are dependent on pH, which may enable the assessment of relative differences in pH between tissue regions. These examples do not use exogenous CEST MRI contrast agents; therefore, we refer to other excellent reviews about endogenous CEST MRI rather than extend our review beyond exogenous agents (49, 50).

4.1. CEST Mechanism

CEST is a simple mechanism that has evolved from NMR spectroscopy (51). A low-power radiofrequency pulse is applied at the specific MR frequency of a proton on a contrast agent (Figure 5*a*). This causes the net coherent magnetization of the proton to be eliminated, a condition known as saturation. When the saturated proton undergoes chemical exchange with a proton on a nearby water molecule, then the saturation is transferred to water while an unsaturated proton is transferred to the agent. This process can be repeated during a long radiofrequency pulse when the agent has a labile proton with a fast chemical exchange rate with water, causing a concentration of several molar of water protons to become saturated from chemical exchange with only millimolar concentrations of the agent. Finally, the MR signal from the remaining unsaturated water protons is detected using standard MRI acquisition methods.

The CEST MRI experiment can be repeated with a radiofrequency saturation pulse iteratively applied over a range of MR frequencies to create a CEST spectrum (Figure 5*c*) (52). This spectrum is referenced to the MR frequency of water at 0 ppm; thus, the decrease in the water signal at 0 ppm of the CEST spectrum arises from direct saturation of water. More importantly, the decrease in water signal at other parts-per-million values represents a CEST effect. The amplitude of the CEST signal is typically used as the quantitative CEST

measurement, although the MR frequency, width of the CEST peak, and other variations that process the CEST spectrum have been used to quantify the CEST effect (53–56).

Paramagnetic CEST agents, also known as paraCEST agents, use a paramagnetic ion within a macrocyclic chelate to shift the MR frequency of labile protons of the agent to values that can range from +500 to −720 ppm from the MR frequency of water (57). These large frequencies greatly facilitate selective saturation of the labile proton of the agent relative to direct saturation of water. Furthermore, the chemical exchange rate (in units of hertz) must be less than the MR frequency of the agent (also in units of hertz). Therefore, paraCEST agents can have faster chemical exchange rates that can transfer more saturation to water during a CEST MRI protocol, which improves the detection sensitivity of the agent. Diamagnetic CEST agents, known as diaCEST agents, have MR frequencies that are relatively close to the frequency of water. This limits the chemical exchange rate of the agent and reduces detection sensitivity. To offset this limitation, biocompatible CEST agents that can be administered at very high concentrations in the ~0.1–1-M range are often used for in vivo CEST MRI studies (58, 59).

4.2. Pharmacokinetic CEST Agents

Exogenous injectable biomaterials such as hydrogels have significant pharmaceutical applications and can enhance stem cell therapy, because they offer a noninvasive, site-specific delivery method into tissues. These biomaterials degrade over time, which can be noninvasively monitored in vivo using CEST MRI. For example, GelinS is a denatured type 1 collagen that has shown good CEST contrast from the amide protons in vivo, and a significant decrease in the CEST signal over 7 days in mouse brain has provided an important understanding of local gel decomposition and tissue clearance (60). The alteration of hydrogel properties such as macromer concentration can result in a change of CEST contrast as observed with a HeMA-HA hydrogel where the exchangeable hydroxyl protons rather than amide protons on HA were detected using CEST MRI in vitro and ex vivo to specifically image and distinguish between different injectable materials (61).

Reporter genes can be applied in the field of imaging to track the pharmacokinetics of cells. CEST MRI-based reporter genes have the added advantage of being biocompatible, do not interfere with T_1 or T_2 MRI contrast mechanisms, and can highlight multiple cells or expression of multiple genes in a CEST MR image. For example, 5-MDHT is a CEST MRI reporter gene probe that was recently synthesized and successfully demonstrated to image HSV1-tk reporter gene expression in a brain tumor model (62). Another recent example involves superpositively charged mutants of green fluorescent protein that produce improved CEST MRI contrast and hence can function as a bimodal reporter gene (63).

4.3. Responsive CEST Agents

Contrast agents that change their detectable MR properties while interacting with a biomarker are often called responsive agents to distinguish these agents from nonresponsive tracer agents. These responsive agents were historically called smart contrast agents, but this anthropomorphic term has been discouraged for descriptions of a chemical entity. Responsive agents have also been called activatable agents. Yet some agents decrease their

detectable signal after interacting with a biomarker, which could be considered as a deactivatable agent. Thus, the MRI contrast agent research field has evolved to refer to these agents as responsive agents. Responsive CEST agents change their chemical shift and/or chemical exchange rate after interacting with a biomarker, which changes the detectable CEST signal from the agent.

4.3.1. Enzyme detection—Enzymes form an important class of cancer biomarkers because their activity can be the signature marker for many metabolic pathways. Enzymatic activity is catalytic; hence, MRI contrast agents that interrogate enzyme activity have the added advantage of increased sensitivity and selectivity because the detection mechanism is agent limited rather than target limited. Usually, the observed changes in the contrast can be unambiguously attributed to the enzyme activity, thus resulting in high specificity. Even a low nanomolar concentration of enzyme can quickly catalyze changes in a millimolar concentration of the modified contrast agent, which results in an amplification of the sensitivity of the CEST MRI signal.

Changes in the chemical structure of a paraCEST agent upon enzyme action result in the appearance of a new CEST signal or the disappearance or change in magnitude of an existing CEST signal. Proteases are good targets for paraCEST agents. For example, an agent based on Tm-DOTA with a peptide substrate of caspase-3 displayed disappearance of the CEST signal after enzyme cleavage, which was attributed to the hydrolysis of the amide bond by the enzyme (64, 65). The agent showed good selectivity for caspase-3 over caspase-8 and good sensitivity of nanomolar enzyme detection. By changing the peptide ligand of such agents, the agent can serve as a platform technology for the detection of other protease enzymes. Recently, a CEST agent has been shown to detect the catalytic activity of transglutaminase, a reverse protease, by detecting the formation of an amide chemical bond from an amine (Figure 5*b*) (66). Other enzyme-responsive paraCEST agents include a Yb(III) chelate with a β-galactose ligand that generates CEST after β-galactosidase cleaves the agent's ligand (67). The CEST effect originates from the formation of the amine group after aromatic delocalization of the phenoxide electron pair. In another example, a paraCEST agent that uses a Yb(III) chelate with an ester group and capped trimethyl lock moiety can detect esterase activity through the appearance of a CEST signal from an amine group generated from an intramolecular lactonization (68).

Recently, diaCEST agents have also been employed to detect enzyme activity, because these nonmetallic agents have the advantage of low toxicity. For example, 5- fluorocytosine can detect cytosine deaminase when the agent is enzymatically converted to 5-fluorouracil, exhibiting a loss of CEST signal during the conversion (69). The 5-fuorouracil can act as a therapeutic agent, so it can be used to track enzyme-based prodrug therapy in tumors. In another example, protein kinase A activity can be detected with an $(LRRASLG)_8$ peptide that acts as a diaCEST MRI contrast agent, because the CEST effect of the peptide is reduced when this kinase enzyme phosphorylates the serine amino acid residue of the peptide (70). In yet another example, a kinase enzyme can phosphorylate a protamine-based CEST agent, which alters CEST contrast as a result of a change in chemical exchange rate or agent conformation during phosphorylation of the protamine (71). Although this method can

detect a small concentration of enzyme because it is not target limited, a high concentration of diaCEST agent is still required for this agent-limited approach.

4.3.2. Detection of metabolites—Recently, CEST MRI has been used to detect several important metabolites, including glucose, glutamate, myoinositiol, creatinine, and hydrogen peroxide. This technique has an advantage over other imaging methods because it allows for the detection and uptake of a metabolically active compound in physiological quantities. For example, the uptake of glucose in a tumor tissue and its metabolism by the tumor cells can be monitored using glucoCEST. These studies have been performed in vivo and can help to distinguish tumor types with different metabolic characteristics (72). Similarly, glucoCEST MRI can monitor the CEST effect from the glutamate amine proton to measure relative glutamate concentrations in the brain and thus can evaluate its potential as a biomarker for treatment of disorders in the central nervous system (73). Another abundant metabolite in the human brain is myoinositol, which is upregulated in several brain disorders. The hydroxyl proton on this metabolite produces a CEST signal, and MICEST MR image contrast was detected in clinical brain studies at high 7-T magnetic field strengths (74). CEST MRI has also detected creatinine concentration in muscle (75). Such detection would be helpful in noninvasive monitoring of the changes in creatinine concentration, thus contributing to the diagnosis of various muscular disorders.

4.3.3. Detection of hypoxia and redox status—The detection of imbalanced in vivo redox environments can help to mark a disease state. A redox imbalance can be triggered by hypoxia. The development of probes that can help to assess oxygen levels and the corresponding redox environment of tumor tissues would be helpful in making treatment decisions. For example, a Co(II) complex shows a CEST signal from the pyrazole NH of the TPT ligand bound to the cobalt ion, with a large paramagnetic proton shift. This signal is lost once the complex is oxidized to a Co(III) complex (76). Such metal complexes can therefore be used to assess the redox environment in tissues.

4.3.4. Detection of ions—Metal ions play an important role in biochemical signaling pathways, and metal homeostasis forms an important subject of medical research with regard to neurodegenerative diseases. Several responsive MRI contrast agents have been devised to study metal ions within in vivo tissue. As an example, the pyridine ligands on a paraCEST agent can coordinate Zn^{2+} in an orientation that leads to an overlap between the bound water molecule and the Zn^{2+} ion. This causes a loss in CEST signal from the agent owing to an accelerated exchange rate of the water molecule (77). An electronic redistribution in a paraCEST agent can also result in a complete loss of CEST signal, as observed in the bis-carboxylate coordination Ca^{2+} complex (78). Thus, an understanding of the bioinorganic chemistry and biomedical imaging can help to develop such CEST agents for metal ion detection.

4.3.5. Measurement of pH—Extracellular pH measurement and monitoring pH alteration are important for clinical diagnoses of various diseases including renal failure, ischemia, and chronic obstructive pulmonary disease. Increased lactic acid secretion and reduced bicarbonate levels within tumor tissues lead to high acidity in those tissues. Measuring

altered pH is relevant for developing therapies that are effective in tissues. An ideal pH-responsive CEST agent should be able to measure the entire physiological pH range from 6.0 to 8.0. The amplitude of CEST signal depends on pH because the chemical exchange between water and an amide or amine proton is base catalyzed at physiological pH.

Many paraCEST agents have been developed to measure pH. For example, the Eu(III) DO3A-tris amide complex can image pH in a ratiometric fashion where the CEST peak exhibits a 5-ppm shift upon deprotonation of the phenolic proton in the pH range of 6.0 to 7.6, resulting in quinone formation (79). Clinically approved iopamidol has two types of amide proton pools with pH-dependent exchange rates that have been exploited to assess in vivo pH in kidneys (80, 81). In another example, extracellular pH was measured using the change in line width of the CEST effect from the amide proton in Tm(III)-DOTAM-Gly-Lys (82). The accuracy of the pH measurement was improved because the CEST effects were insensitive to changes in concentration and temperature.

4.3.6. Measurement of temperature—An increase in temperature often causes the chemical exchange rate to increase. As the chemical exchange rate approaches the difference in MR frequency between water and the amide's proton, a phenomenon known as MR coalescence causes the detected MR frequency of the agent to decrease. Therefore, monitoring the MR frequency of the CEST peak can be used to measure temperature. Within the field of CEST agents, this measurement of temperature has so far been achieved only using paraCEST agents. For example, a Yb(III)-HbDO3A agent has been used to detect temperature by monitoring the shift in the CEST peak from the hydroxyl groups with change in temperature (83). Indeed, this probe has been used to assess both pH and temperature.

5. CONTRAST AGENTS FOR MR SPECTROSCOPY AND SPECTROSCOPIC IMAGING

5.1. ^{13}C Hyperpolarization Mechanism

The detection of ^{13}C, an MRI-active isotope of carbon, has been a staple of biological NMR spectroscopy, including ^{13}C NMR studies of natural products, polymers for biomedical research, and biomolecules such as proteins and nucleic acids (84). However, ^{13}C MR spectroscopy (MRS) has been more challenging to apply to in vivo biomedical studies owing to the low 1.1% abundance of ^{13}C among all carbon atoms, the lower detection sensitivity of ^{13}C compared with ^{1}H, and the lower concentration of mobile ^{13}C in the body relative to the high concentration of mobile ^{1}H content in tissue water (note that ^{13}C in the solid state in tissues has very fast relaxation and broad chemical shift anisotropy, rending solid-state ^{13}C impractical for in vivo detection). For these reasons, ^{13}C MRS has been difficult to perform during preclinical in vivo studies and has not become a routine tool in the clinic (85). The corollary of ^{13}C magnetic resonance spectroscopic imaging (MRSI), whereby a ^{13}C MR spectrum is generated for each two-dimensional (2D) pixel or 3D voxel within an image, has had a similar fate as a result of detection sensitivity (86).

To overcome this challenge, recent advances have developed hyperpolarized ^{13}C contrast agents, which produce as much as 10,000-fold greater ^{13}C signal than do endogenous

biomolecules with natural ^{13}C polarization (87). The most practical method for generating hyperpolarized ^{13}C agents for in vivo studies uses dynamic nuclear polarization (DNP) (88). This process rapidly freezes a mixture of a stable trityl radical with the material to be polarized. When placed in a strong magnetic field at 3 T to 5 T and maintained cold at 1 to 5 K, almost all the magnetic moments of the radical's unpaired electron are aligned with the magnetic field, thereby creating a hyperpolarized state. The magnetic moment of the radical's electron is more than 2,600 times greater than the magnetic moment of a carbon atom; thus, this hyperpolarized state of the electron is relatively large. This hyperpolarization is then transferred to the ^{13}C nucleus using microwave radiation close to the MR frequency of the electron spin. After achieving hyperpolarization, the frozen sample must be rapidly dissolved and heated to physiological temperature before being administered to an animal model or a patient. This process typically uses a superheated solvent at 180°C and 10 bar.

Several chemical modifications have been used to improve this process. For example, glycerol or dimethylsulfoxide can be used to reduce crystallization during the initial freezing process that should form an amorphous glass. Gd^{3+} ions can be added to the sample to promote rapid T_1 relaxation of the electron and accelerate the transfer rate of dynamic nuclear polarization, which can improve hyperpolarization by 1.5- to 10-fold (89). Although the trityl radical has an electron paramagnetic resonance line width that is very appropriate for hyperpolarization of ^{13}C, other radicals such as nitroxides or a mixture of radicals produced by UV radiation of the sample have also been used, especially for hyperpolarization of other nuclei (90). An alternative method of polarization, termed parahydrogen-induced polarization, can also be used to hyperpolarize ^{13}C (91). However, this method requires chemical symmetry, which has limited the use of this technique for biomedical imaging studies. To date, only the symmetrical succinate molecule has been successfully hyperpolarized for in vivo studies, although recent results with symmetrical molecules that can then be rapidly converted to asymmetrical metabolites have shown promise (92, 93). Yet another alternative approach uses signal amplification by reversible exchange (SABRE), which uses a metallic catalyst to transfer polarization from parahydrogen to a contrast agent (94). Although SABRE can very rapidly polarize a sample within a few seconds, the level of polarization is typically less than 10% compared with 30–40% polarization achieved after a few hours with DNP. Thus, DNP is still the method of choice for current in vivo hyperpolarized ^{13}C studies.

The major weakness of hyperpolarized ^{13}C MRI is the T_1 relaxation rate of the ^{13}C, which causes the loss of the hyperpolarized state. The T_1 relaxation process can be slowed by storing the hyperpolarization in a singlet state, reducing chemical anisotropy at the carbon position and/or replacing hydrogen atoms with deuterons to eliminate ^{1}H-^{13}C coupling (95, 96). Careful experimental designs have resulted in ^{13}C T_1 relaxation time constants as long as 60 s, although T_1 relaxation time constants of 20 to 30 s are sufficient for practical in vivo studies. Yet this short time frame limits the study of in vivo hyperpolarized ^{13}C to molecules that are involved in rapid catabolic reactions related to energy metabolism, rather than slower anabolic pathways that are related to biosynthesis. As an additional complication, the excitation and MR detection of hyperpolarized ^{13}C nuclei also cause their hyperpolarization

to be lost, requiring clever MRI protocols that iteratively sample small populations of the nuclei during temporal studies (97).

5.2. Hyperpolarized ^{13}C MRS/I Agents

MRS/I of many ^{13}C hyperpolarized agents have been used to interrogate cell metabolism, particularly in animal tumor models and in patients with prostate cancer, with some studies performed with cardiovascular tissues. Hyperpolarized [1-^{13}C]pyruvate has been the most commonly used metabolite for cancer studies (Figure 6) (98). In particular, monocarboxylate transporters carry pyruvate into the cell, lactate dehydrogenase converts pyruvate to lactate, and alanine aminotransferase converts pyruvate to alanine, all of which are upregulated in tumor cells. For comparison, [2-^{13}C]pyruvate has been used to assess enzyme activities in the Krebs cycle (99). In addition, hyperpolarized pyruvate has been used to detect metabolism associated with carbonic anhydrase, mitogen-activated protein kinase, and choline kinase α (100–102). Similarly, the ^{13}C-hyperpolarized metabolites lactate, alanine, [5-^{13}C]glutamine, 1-keto[1-^{13}C]isocaproate, diethyl[1-^{13}C]succinate, [2-^{13}C]fructose, and 3,5-diflurorbenzoylglutamic acid have been used to evaluate biochemical pathways (103–107). Importantly, the metabolic energy pathways are highly interconnected. Therefore, the catabolism of each of these metabolites may be unexpectedly sensitive to changes in one small part of the metabolic network. Considerable care must thus be taken to adequately assess the metabolic profile of the pathological tissue. For example, injection of a high nonphysiological concentration of hyperpolarized pyruvate can cause an imbalance to the metabolic network, which must be considered during quantitative studies.

As described above, the extracellular pH of the tumor microenvironment is a useful biomarker for improving tumor diagnoses and selecting chemotherapies for precision medicine. Tumor pH can be measured using hyperpolarized bicarbonate, $H^{13}CO_3^-$, which undergoes rapid interconversion with carbon dioxide, $^{13}CO_2$, via carbonic anhydrase enzyme activity (108). The ratio of bicarbonate to carbon dioxide concentrations can be detected with MRS/I and then used to determine pH through the Henderson-Hasselbalch equation. Unlike studies of metabolism, this pH determination must be detected at steady-state equilibrium between bicarbonate and carbon dioxide that takes time to establish (109). This time may not be available if the T_1 relaxation time constant of bicarbonate is short or if carbonic anhydrase activity is insufficiently fast. Importantly, carbonic anhydrase works more slowly in acidic conditions such as the tumor extracellular environment, which causes tumor pH to be overestimated (tumor acidosis is underestimated), thereby reducing the utility of this method. This complication once again demonstrates that considerable care must be taken to adequately assess the metabolic dependencies of hyperpolarized ^{13}C studies.

Hyperpolarized ^{13}C can also evaluate the redox state of tumors and other tissues by monitoring the intracellular reduction of dehydroascorbate to form ascorbate (vitamin C) (110, 111). The long T_1 relaxation time of dehydroascorbate greatly facilitates in vivo MRS/I studies. The rate of DHA conversion to ascorbate may indicate the tumor's capacity to resist oxidative stress, which can affect treatment decisions regarding radiotherapy and chemotherapy. However, the high nonphysiological concentrations of dehydroascorbate that

must be administered to produce detectable MRS/I results have been shown to cause respiratory suppression, which impedes clinical translation of this approach. This complication further demonstrates that the fate of the metabolic network, rather than a single metabolic step, must be considered during assessments of hyperpolarized ^{13}C MRS/I studies.

6. FUTURE DIRECTIONS AND REMAINING CHALLENGES

Despite the strong progress made in developing new types of MRI contrast agents, more research is needed to translate these agents into clinical practice. The clinical translation of molecular imaging is often hampered by the substantial technical expertise required to interpret results that arise from molecular compositions in tissues, relative to interpreting anatomical or functional imaging tests. T_{2ex}, CEST, and hyperpolarized ^{13}C MRI contrast agents are designed to provide simplicity during imaging by providing a ratio of MR signals that is sensitive to the biomarker and insensitive to other environmental effects in tissues. For example, this ratio is independent of the concentration of the agent in tissue, avoiding a major complication when interpreting other types of molecular imaging results. Yet this ratiometric approach needs to be tested and validated in clinical trials for each of these types of new MRI contrast agents.

As another challenge, toxicology studies are critical for ensuring biomedical safety during clinical trials. Yet funding for toxicology studies of imaging contrast agents can be difficult to secure, which is exacerbated by the high cost and long time frames of most common in vivo toxicology tests. Moreover, the revenue for clinically-approved molecular imaging agents is a fraction of the revenue generated by clinically-approved pharmaceuticals, partly due to the single or infrequent use of imaging agents relative to daily or frequent drug administrations. This lower revenue dampens enthusiasm for initial investments in toxicological tests. A potential solution to this challenge is to tie the molecular imaging agent to the pharmaceutical drug, whereby the drug is only prescribed to a patient if the molecular imaging test is positive. This ties the development costs of the imaging agent to the profitability of the drug. Although this approach may appear to burden the development of new drug entities, linking the imaging diagnosis with the therapy contributes to the drive toward personalized medicine that matches the best drug and drug regimen for each individual patient.

Acknowledgments

The authors acknowledge support from the National Institute for Biomedical Imaging and Bioengineering of the National Institutes of Health (R01CA167183, R01, R01) and the Phoenix Friends of the University of Arizona Cancer Center.

LITERATURE CITED

1. Weissleder, R.; Ross, BD.; Rehemtulla, R.; Gambhir, SS., editors. Molecular Imaging: Principles and Practice. Shelton, CT: People’s Med. Pub. House; 2010.
2. Ahrens ET, Rothbacher U, Jacobs RE, Fraser SE. A model for MRI contrast enhancement using T_1 agents. PNAS. 1998; 95:8443–48. [PubMed: 9671697]

3. Mills PH, Ahrens ET. Theoretical MRI contrast model for T_2 agents. Magn Reson Med. 2007; 57:442–47. [PubMed: 17260382]
4. Ali MM, Liu G, Shah T, Flask CA, Pagel MD. Using two chemical exchange saturation transfer magnetic resonance imaging contrast agents for molecular imaging studies. Acc Chem Res. 2008; 42:915–24. [PubMed: 19514717]
5. Nelson SJ, Ozhinsky E, Li Y, Park IW, Crane J. Strategies for rapid in vivo ^{1}H and hyperpolarized ^{13}C MR spectroscopic imaging. J Magn Reson. 2013; 229:187–97. [PubMed: 23453759]
6. Dua P, Chaudhari KN, Lee C-H, Chaudhari NK, Song S-W, et al. Evaluation of toxicity and gene expression changes triggered by oxide nanoparticles. Bull Korean Chem Soc. 2011; 32:2051–57.
7. Allen MJ, MacRenaris KW, Venkatasubramanian PN, Meade TJ. Cellular delivery of MRI contrast agents. Chem Biol. 2004; 11:301–7. [PubMed: 15123259]
8. Yoo B, Pagel MD. An overview of responsive MRI contrast agents for molecular imaging. Front Biosci. 2008; 13:1733–52. [PubMed: 17981664]
9. Hingorani DV, Bernstein AS, Pagel MD. A review of responsive MRI contrast agents: 2005–2014. Contrast Media Mol Imaging. 2014; 10:245–65. [PubMed: 25355685]
10. Hingorani DV, Yoo B, Bernstein AS, Pagel MD. Detecting enzyme activities with exogenous MRI contrast agents. Chem Eur J. 2014; 20:9840–50. [PubMed: 24990812]
11. Bulte, JWM.; Kraitchman, DL.; Ben-Hur, T. Use of iron oxide MR contrast agents for monitoring stem cell therapy. In: Greer, DA., editor. Focus on Stem Cell Research. Hauppauge, NY: Nova Sci; 2004. p. 1-32.
12. Ferrauto G, Delli Castelli D, Di Gregorio E, Langereis S, Burdinski D, et al. Lanthanide-loaded erythrocytes as highly sensitive chemical exchange saturation transfer MRI contrast agents. J Am Chem Soc. 2014; 136:638–41. [PubMed: 24359116]
13. Terreno E, Cabella C, Carrera C, Delli Castelli D, Mazzon R, et al. From spherical to osmotically shrunken paramagnetic liposomes: an improved generation of LIPOCEST MRI agents with highly shifted water protons. Angew Chem Int Ed. 2007; 46:966–68.
14. Ali MM, Yoo B, Pagel MD. Tracking the relative in vivo pharmacokinetics of nanoparticles with PARACEST MRI. Mol Pharm. 2009; 6:1409–16. [PubMed: 19298054]
15. Davis TW, O'Neal JM, Pagel MD, Zweifel BS, Mehta PP, et al. Synergy between celecoxib and radiotherapy results from inhibition of COX-2-derived PGE2, a survival factor for tumor and associated vasculature. Cancer Res. 2004; 64:279–85. [PubMed: 14729635]
16. Kassner A, Thornhill R. Measuring the integrity of the human blood-brain barrier using magnetic resonance imaging. Methods Mol Biol. 2011; 686:229–45. [PubMed: 21082374]
17. Brown, RW.; Cheng, Y-CN.; Haake, EM.; Thompson, MR.; Venkatesan, R., editors. Magnetic Resonance Imaging: Physical Principles and Sequence Design. 2. Hoboken NJ: Wiley; 2014.
18. Carr DH, Brown J, Bydder GM, Weinmann H-J, Speck U, et al. Intravenous chelated gadolinium as a contrast agent in NMR imaging of cerebral tumours. Lancet. 1984; 1:484–86. [PubMed: 6142210]
19. Edelman RR, Mattle HP, Atkinson DJ, Hill T, Finn JP, et al. Cerebral blood flow: assessment with dynamic contrast-enhanced T_2^*-weighted MR imaging at 1.5 T. Radiologica. 1990; 176:211–20.
20. Carr DH, Brown J, Bydder GM, Steiner RH, Weinmann HJ, et al. Gadolinium-DTPA as a contrast agent in MRI: initial clinical experience in 20 patients. Am J Roentgenol. 1984; 143:215–24. [PubMed: 6611046]
21. Fiel RJ, Button TM, Gilani S, Mark EH, Musser DA, et al. Proton relaxation enhancement by manganese(III)$TPPS_4$ in a model tumor system. Magn Reson Imaging. 1987; 5:149–56. [PubMed: 3586881]
22. Laurent, S.; Vander Elst, L.; Muller, RN. Superparamagnetic iron oxide nanoparticles for MRI. In: Merbach, A.; Helm, L.; Toth, E., editors. Chemistry of Contrast Agents in Medical Magnetic Resonance Imaging. Hoboken, NJ: Wiley; 2013. p. 427-47.
23. Kunjachan S, Ehling J, Storm G, Kiessling F, Lammers T. Noninvasive imaging of nanomedicines and nanotheranostics: principles, progress, and prospects. Chem Rev. 2015; 115:10907–37. [PubMed: 26166537]
24. Kuo PH, Kanal E, Abu-Alfa AK, Cowper SE. Gadolinium-based MR contrast agents and nephrogenic systemic fibrosis. Radiology. 2007; 242:647–49. [PubMed: 17213364]

25. Dydak U, Criswell SR. Imaging modalities for manganese toxicity. Issues Toxicol. 2015; 22:477–512.
26. Lee H, Yoo D, Ling D, Cho MH, Hyeon T, Cheon J. Iron oxide based nanoparticles for multimodal imaging and magnetoresponsive therapy. Chem Rev. 2015; 115:10637–89. [PubMed: 26250431]
27. Sipkins DA, Cheresh DA, Kazemi MR, Nevin LM, Bednarksi MD, Li KCP. Detection of tumor angiogenesis in vivo by $\alpha_v\beta_3$-targeted magnetic resonance imaging. Nat Med. 1998; 4:623–26. [PubMed: 9585240]
28. Anderson SA, Rader RK, Westlin WF, Null C, Jackson D, et al. Magnetic resonance contrast enhancement of neovasculature with $\alpha_v\beta_3$-targeted nanoparticles. Magn Reson Med. 2000; 44:433–39. [PubMed: 10975896]
29. Hilger I, Trost R, Reichenbach JR, Linss W, Lisy M-R, et al. MR imaging of Her-2/neu protein using magnetic nanoparticles. Nanotechnology. 2007; 18:135103. [PubMed: 21730374]
30. Kinoshita M, Yoshioka Y, Okita Y, Hashimoto N, Yoshimine T. MR molecular imaging of HER-2 in a murine tumor xenograft by SPIO labeling of anti-HER-2 affibody. Contrast Media Mol Imaging. 2010; 5:18–22. [PubMed: 20140973]
31. Frullano L, Catana C, Benner T, Sherry AD, Caravan P. Bimodal MRI-PET agent for quantitative pH imaging. Angew Chem Int Ed. 2010; 49:2382–84.
32. Jing L, Ding K, Kershaw SV, Kempson IM, Rogach AL, Gao M. Magnetically engineered semiconductor quantum dots as multimodal imaging probes. Adv Mater. 2014; 26:6367–86. [PubMed: 25178258]
33. Lee S, Chen X. Dual-modality probes for molecular imaging. Mol Imaging. 2009; 8(2):87–100. [PubMed: 19397854]
34. Pagel MD. The hope and hype of multimodality imaging contrast agents. Nanomedicine. 2011; 6:945–48. [PubMed: 21955073]
35. Raghunand N, Zhang S, Sherry AD, Gillies RJ. In vivo magnetic resonance imaging of tissue pH using a novel pH-sensitive contrast agent, GdDOTA-$_4$AmP. Acad Radiol. 2002; 9:S481–83. [PubMed: 12188315]
36. Esqueda AC, López JA, Andreu-de-Riguer G, Alvarado-Monzón JC, Ratnakar J, et al. A new gadolinium based MRI zinc sensor. J Am Chem Soc. 2009; 131:11387–91. [PubMed: 19630391]
37. Vold RL, Daniel AS, Chan SO. Magnetic resonance measurements of proton exchange in aqueous urea. J Am Chem Soc. 1970; 92:6771–76.
38. Granot J, Fiat D. Effect of chemical exchange on the transverse relaxation rate of nuclei in solution containing paramagnetic ions. J Magn Reson. 1974; 15:540–48.
39. Aime S, Nano R, Grandi M. A new class of contrast agents for magnetic resonance imaging based on selective reduction of water-T_2 by chemical exchange. Invest Radiol. 1988; 23:S267–70. [PubMed: 3198360]
40. Soesbe TC, Merritt ME, Green KN, Rojas-Quijano FA, Sherry AD. T_2 exchange agents: a new class of paramagnetic MRI contrast agent that shortens water T_2 by chemical exchange rather than relaxation. Magn Reson Med. 2011; 66:1697–703. [PubMed: 21608031]
41. Sherry AD, Wu Y. The importance of water exchange rates in the design of responsive agents for MRI. Curr Opin Chem Biol. 2013; 17:167–74. [PubMed: 23333571]
42. Geraldes, CFGC. Lanthanide shift reagents. In: Atwood, DA., editor. The Rare Earth Elements: Fundamentals and Applications. Hoboken, NJ: Wiley; 2012. p. 501-20.
43. Soesbe TC, Ratnakar SJ, Milne M, Zhang S, Do QN, et al. Maximizing T_2-exchange in Dy^{3+}DOTA-(amide)$_x$ chelates: fine-tuning the water molecule exchange rate for enhanced T_2 contrast in MRI. Magn Reson Med. 2014; 71:1179–85. [PubMed: 24390729]
44. Yadav NN, Xu J, Bar-Shir A, Qin Q, Chan KWY, et al. Natural D-glucose as a biodegradable MRI relaxation agent. Magn Reson Med. 2014; 72:823–28. [PubMed: 24975029]
45. Daryaei I, Pagel MD. New type of responsive MRI contrast agent that modulates T_{2ex} relaxation: detection of nitric oxide. Proc Am Chem Soc. 2014; 247:498. (Abstr.).
46. Cai K, Haris M, Singh A, Kogan F, Greenberg JH, et al. Magnetic resonance imaging of glutamate. Nat Methods. 2012; 18:302–6.

47. Kogan F, Haris M, Debrosse C, Sing A, Nanga RP, et al. In vivo chemical exchange saturation transfer imaging of creatine (CrCEST) in skeletal muscle at 3T. J Magn Reson Imaging. 2014; 40:596–602. [PubMed: 24925857]
48. Ling W, Regatta RR, Navon G, Jerschow A. Assessment of glycosaminoglycan concentration *in vivo* by chemical exchange-dependent saturation transfer (gagCEST). PNAS. 2008; 105:2266–70. [PubMed: 18268341]
49. Vinogradov E, Sherry AD, Lenkinski RE. CEST: from basic principles to applications, challenges, and opportunities. J Magn Reson. 2013; 229:155–72. [PubMed: 23273841]
50. Dula AN, Smith SA, Gore JC. Application of chemical exchange saturation transfer (CEST) MRI for endogenous contrast at 7 Tesla. J Neuroimaging. 2013; 23:526–32. [PubMed: 23402307]
51. Ward KM, Aletras AH, Balaban RS. A new class of contrast agents for MRI based on proton chemical exchange dependent saturation transfer (CEST). J Magn Reson. 2000; 143:79–87. [PubMed: 10698648]
52. Bryant RG. The dynamics of water-protein interactions. Annu Rev Biophys Biomol Struct. 1996; 25:29–53. [PubMed: 8800463]
53. Sheth VR, Liu G, Li Y, Pagel MD. Improved pH measurements with a single PARACEST MRI contrast agent. Contrast Media Mol Imaging. 2012; 7:26–34. [PubMed: 22344877]
54. Wang X, Wu Y, Soesbe TC, Yu J, Zhao P, et al. A pH-responsive MRI agent that can be activated beyond the tissue magnetization transfer window. Angew Chem Int Ed. 2015; 54:8662–64.
55. McVicar, Li AX, Suchy M, Hudson RM, Menon RS, Bartha R. Simultaneous in vivo pH and temperature mapping using a PARACEST-MRI contrast agent. Magn Reson Med. 2013; 70:1016–25. [PubMed: 23165779]
56. Tereno E, Stancanello J, Longo D, Delli Castelli D, Milone L, et al. Methods for an improved detection of the CEST MRI effect. Contrast Media Mol Imaging. 2009; 4:237–47. [PubMed: 19839029]
57. Viswanathan S, Kovacs Z, Green KN, Ratnakar SJ, Sherry AD. Alternatives to gadolinium-based metal chelates for magnetic resonance imaging. Chem Rev. 2010; 110:2960–3018. [PubMed: 20397688]
58. Moon BF, Jones KM, Chen LQ, Liu P, Randtke EA, et al. A comparison of iopromide and iopamidol, two acidoCEST MRI contrast media that measure tumor extracellular pH. Contrast Media Mol Imaging. 2015; 10:446–55. [PubMed: 26108564]
59. Chan KY, McMahon MT, Kato Y, Liu G, Bulte JWM, et al. Natural D-glucose as a biodegradable MRI contrast agent for detecting cancer. Magn Reson Med. 2012; 68:1764–73. [PubMed: 23074027]
60. Liang Y, Bar-Shir A, Song X, Gilad AA, Walczak P, Bulte JWM. Label-free imaging of gelatin-containing hydrogel scaffolds. Biomaterials. 2015; 42:144–50. [PubMed: 25542802]
61. Dorsey SM, Haris M, Singh A, Witschey WRT, Rodell CB, Kogan F. Visualization of injectable hydrogels using chemical exchange saturation transfer MRI. ACS Biomater Sci Eng. 2015; 1:227–37.
62. Bar-Shir A, Liu G, Greenberg MW, Bulte JWM, Gilad AA. Synthesis of a probe for monitoring HSV1-tk reporter gene expression using chemical exchange saturation transfer MRI. Nat Protoc. 2013; 8:2380–91. [PubMed: 24177294]
63. Bar-Shir A, Liang Y, Chan KWY, Gilad AA, Bulte JWM. Supercharged green fluorescent proteins as bimodal reporter genes for CEST MRI and optical imaging. Chem Commun. 2015; 51:4869–71.
64. Yoo B, Pagel MD. A PARACEST MRI contrast agent to detect enzyme activity. J Am Chem Soc. 2006; 128:14032–33. [PubMed: 17061878]
65. Yoo B, Raam MS, Rosenblum RM, Pagel MD. Enzyme-responsive PARACEST MRI contrast agents: a new biomedical imaging approach for studies of the proteasome. Contrast Media Mol Imaging. 2007; 2:189–98. [PubMed: 17712869]
66. Hingorani DV, Randtke EA, Pagel MD. A catalyCEST MRI contrast agent that detects the enzyme-catalyzed creation of a covalent bond. J Am Chem Soc. 2013; 135:6396–98. [PubMed: 23601132]
67. Chauvin T, Durand P, Bernier M, Meudal H, Doan B-T, et al. Detection of enzymatic activity by PARACEST MRI: a general approach to target a large variety of enzymes. Angew Chem Int Ed. 2008; 47:4370–72.

68. Li Y, Sheth VR, Liu G, Pagel MD. A self-calibrating PARACEST MRI contrast agent that detects esterase enzyme activity. Contrast Media Mol Imaging. 2011; 6:219–28. [PubMed: 21861282]
69. Liu G, Liang Y, Bar-Shir A, Chan KWY, Galoththawela CS, et al. Monitoring enzyme activity using a diamagnetic chemical exchange saturation transfer magnetic resonance imaging contrast agent. J Am Chem Soc. 2011; 133:16326–29. [PubMed: 21919523]
70. Airan RD, Bar-Shir A, Liu G, Pelled G, McMahon MT, et al. MRI biosensor for protein kinase A encoded by a single synthetic gene. Magn Reson Med. 2012; 68:1919–23. [PubMed: 23023588]
71. Oskolkov N, Bar-Shir A, Chan KWY, Song X, van Zinjl PCM, et al. Biophysical characterization of human protamine-1 as a responsive CEST MR contrast agent. ACS Macro Lett. 2014; 4:34–38. [PubMed: 25642384]
72. Walker-Samuel S, Ramasawmy R, Torrealdea F, Rega M, Rajkumar V, et al. *In vivo* imaging of glucose uptake and metabolism in tumors. Nat Med. 2013; 19:1067–72. [PubMed: 23832090]
73. Cai K, Haris M, Kogan F, Greenberg JH, Hariharan H, et al. Magnetic resonance imaging of glutamate. Nat Med. 2012; 18:302–6. [PubMed: 22270722]
74. Haris M, Cai K, Singh A, Hariharan H, Reddy R. *In vivo* mapping of brain myoinositol. Neuroimage. 2011; 54:2079–85. [PubMed: 20951217]
75. Kogan F, Haris M, Singh A, Debrosse C, Nanga RP, et al. Method for high-resolution imaging of creatine in vivo using chemical exchange saturation transfer. Magn Reson Med. 2014; 71:164–72. [PubMed: 23412909]
76. Tsitovich PB, Burns PJ, McKay AM, Morrow JR. Redox-activated MRI contrast agents based on lanthanide and transition metal ions. J Inorg Biochem. 2014; 133:143–54. [PubMed: 24529651]
77. Trokowski R, Ren J, Kálmán FK, Sherry AD. Selective sensing of zinc ions with a PARACEST contrast agent. Angew Chem Int Ed. 2005; 44:6920–23.
78. Angelovski G, Chauvin T, Pohmann R, Logothetis NK, Tóth E. Calcium-responsive paramagnetic CEST agents. Bioorg Med Chem. 2011; 19:1097–105. [PubMed: 20691598]
79. Wu Y, Soesbe TC, Kiefer GE, Zhao P, Sherry AD. A responsive europium(III) chelate that provides a direct readout of pH by MRI. J Am Chem Soc. 2010; 132:14002–3. [PubMed: 20853833]
80. Sheth VR, Li Y, Chen LQ, Howison CM, Flask CA, Pagel MD. Measuring in vivo tumor pHe with CEST-FISP MRI. Magn Reson Med. 2012; 67:760–68. [PubMed: 22028287]
81. Longo DL, Dastru W, Digilio G, Keupp J, Langereis S, et al. Iopamidol as a responsive MRI-chemical exchange saturation transfer contrast agent for pH mapping of kidneys: in vivo studies in mice at 7 T. Magn Reson Med. 2011; 65:202–11. [PubMed: 20949634]
82. McVicar N, Li AX, Suchy M, Hudson RHE, Menon RS, Bartha R. Simultaneous in vivo pH and temperature mapping using a PARACEST-MRI contrast agent. Magn Reson Med. 2013; 70:1016–25. [PubMed: 23165779]
83. Delli Castelli D, Enzo T, Silvio A. YbIII-HPDO3A: a dual pH- and temperature-responsive CEST agent. Angew Chem Int Ed. 2011; 50:1798–800.
84. Breitmaier, E.; Voelter, W. ^{13}C NMR Spectroscopy: Methods and Applications in Organic Chemistry. Weinheim, Ger: Verlag Chemie; 1978.
85. de Graaf RA, Rothman DL, Behar KL. State of the art direct ^{13}C and indirect ^{1}H-[^{13}C] NMR spetroscopy in vivo: a practical guide. NMR Biomed. 2011; 24:958–72. [PubMed: 21919099]
86. Muller S, Beckmann N. ^{13}C spectroscopic imaging: a simple approach to in vivo ^{13}C investigations. Magn Reson Med. 1989; 12(3):400–6. [PubMed: 2628688]
87. Golman K, Ardenkjær-Larsen JH, Petersson JS, Månsson S, Leunbach I. Molecular imaging with endogenous substances. PNAS. 2003; 100:10435–39. [PubMed: 12930896]
88. Ardenkjær-Larsen JH, Fridlund B, Gram A, Hansson G, Hansson L, et al. Increase in signal-to-noise ratio of >10,000 times in liquid-state NMR. PNAS. 2003; 100:10158–63. [PubMed: 12930897]
89. Ardenkjær-Larsen JH, Macholl S, Johannesson H. Dynamic nuclear polarization with trityls at 1.2 K. Appl Magn Reson. 2008; 34:509–22.
90. Eichhorn TR, Takado Y, Salameh N, Capozzi A, Cheng T, et al. Hyperpolarization without persistent radicals for in vivo real-time metabolic imaging. PNAS. 2013; 110:18064–69. [PubMed: 24145405]

91. Duckett SB, Mewis ER. Application of parahydrogen-induced polarization techniques in NMR spectroscopy and imaging. Acc Chem Res. 2012; 45:1247–57. [PubMed: 22452702]
92. Bhattacharya P, Chekmenev EY, Perman WH, Harris KC, Lin A, Norton V. Towards hyperpolarized ^{13}C-succinate imaging of brain cancer. J Magn Reson. 2007; 186:150–55. [PubMed: 17303454]
93. Reineri F, Boi T, Aime S. Parahydrogen induced polarization of ^{13}C carboxylate resonance in acetate and pyruvate. Nat Commun. 2015; 6:5858. [PubMed: 25556844]
94. Pravdivtsev AN, Yurkovskaya AV, Vieth HM, Ivanov K. RF-SABRE: a way to continuous spin hyperpolarization at high magnetic fields. J Phys Chem B. 2015; 119:13619–29. [PubMed: 25970807]
95. Levitt MH. Singlet nuclear magnetic resonance. Annu Rev Phys Chem. 2012; 63:89–105. [PubMed: 22224703]
96. Rodrigues TB, Serrao EM, Kennedy BWC, Hu D-E, Kettunen MI, Brindle KM. Magnetic resonance imaging of tumor glycolysis using hyperpolarized ^{13}C-labeled glucose. Nat Med. 2014; 20:93–97. [PubMed: 24317119]
97. Sriram R, Kurhanewicz J, Vigneron DB. Hyperpolarized carbon-13 MRI and MRS studies. eMagRes. 2014; 3:311–24.
98. Golman K, in ‘t Zandt R, Thaning M. Real-time metabolic imaging. PNAS. 2006; 103:11270–75. [PubMed: 16837573]
99. Barb AW, Hekmatyar SK, Glushka JN, Prestegard JH. Probing alanine transaminase catalysis with hyperpolarized $^{13}CD_3$-pyruvate. J Magn Reson. 2013; 228:59–65. [PubMed: 23357427]
100. Schroeder MA, Ali MA, Hulikova A, Supuran CT, Clarke K, et al. Extramitochondrial domain rich in carbonic anhydrase activity improves myocardial energetics. PNAS. 2013; 110:E958–67. [PubMed: 23431149]
101. Lodi A, Woods MS, Ronen MS. Treatment with the MEK inhibitor U0126 induces decreased hyperpolarized pyruvate to lactate conversion in breast, but not prostate, cancer cells. NMR Biomed. 2013; 26:299–306. [PubMed: 22945392]
102. Venkatesh HS, Chaumeil MM, Ward CS, Haas-Kogan DA, James CD, Ronen SM. Phosphocholine and hyperpolarized lactate provide magnetic resonance biomarkers of PI3K/Akt/mTOR inhibition in glioblastoma. Neuro-Oncology. 2012; 14:315–25. [PubMed: 22156546]
103. Gallagher FA, Kettunen MI, Day SE, Lerche M, Brindle KM. ^{13}C MR spectroscopy measurements of glutaminase activity in human hepatocellular carcinoma cells using hyperpolarized ^{13}C-labeled glutamine. Magn Reson Med. 2008; 60:253–57. [PubMed: 18666104]
104. Karlsson M, Jensen PR, in ‘t Zandt R, Gisselsson A, Hansson G, et al. Imaging of branched chain amino acid metabolism in tumors with hyperpolarized ^{13}C ketoisocaproate. Int J Cancer. 2010; 127:729–36. [PubMed: 19960440]
105. Zacharias NM, Chan HR, Sallasuta N, Ross BR, Bhattacharya P. Real-time molecular imaging of tricarboxylic acid cycle metabolism in vivo by hyperpolarized 1-^{13}C diethyl succinate. J Am Chem Soc. 2011; 134:934–43. [PubMed: 22146049]
106. Keshari KR, Wilson DM, Chen AP, Bok R, Larson PEZ, et al. Hyperpolarized [2-^{13}C]-fructose: a hemiketal DNP substrate for in vivo metabolic imaging. J Am Chem Soc. 2009; 131:17591–96. [PubMed: 19860409]
107. Jamin Y, Gabellieri C, Smyth L, Reynolds S, Robinson SP, et al. Hyperpolarized ^{13}C magnetic resonance detection of carboxypeptidase G2 activity. Magn Reson Med. 2009; 62:1300–4. [PubMed: 19780183]
108. Gallagher FA, Kettunen MI, Day SE, Hu E-D, Ardenkjær-Larsen JH, et al. Magnetic resonance imaging of pH *in vivo* using hyperpolarized ^{13}C-labelled bicarbonate. Nature. 2008; 453:940–43. [PubMed: 18509335]
109. Gallagher FA, Kettunen MA, Brindle MK. Imaging pH with hyperpolarized ^{13}C. NMR Biomed. 2011; 24:1006–15. [PubMed: 21812047]
110. Bohndiek SE, Sai V, Wang ZJ, Vanbrocklin HF, Kurhanewicz J, Wilson DM. Hyperpolarized [1-^{13}C]-ascorbic and dehydroascorbic acid: vitamin C as a probe for imaging redox status in vivo. J Am Chem Soc. 2011; 133:11795–801. [PubMed: 21692446]

111. Keshari KR, Sai V, Wang ZJ, Vanbrocklin HF, Kurhanewica J, Wilson DM. Hyperpolarized [1-^{13}C] dehydroascorbate MR spectroscopy in a murine model of prostate cancer: comparison with ^{18}F-FDG PET. J Nucl Med. 2013; 54:922–28. [PubMed: 23575993]

SUMMARY POINTS

1. T_1 and T_2^* contrast agents have made a significant impact on anatomical imaging, but recent advances of these agents for molecular imaging have been more limited.
2. The recent emergence of T_{2ex} agents provides new capabilities for molecular imaging, particularly by providing new opportunities to develop agents that have slower chemical exchange rates that can be more responsive to molecular biomarkers. Examples of T_{2ex} agents demonstrate their utility for molecular imaging of biomarkers.
3. CEST MRI contrast agents have a slow chemical exchange rate that may be modulated by molecular biomarkers, improving specificity for biomarker detection with molecular imaging. Many recent examples of CEST agents show the advantages of this approach for molecular imaging of biomarkers.
4. Hyperpolarized ^{13}C contrast agents also provide capabilities for detecting specific molecular biomarkers, while also offering the chance to track metabolism with these highly sensitive small-molecule agents.

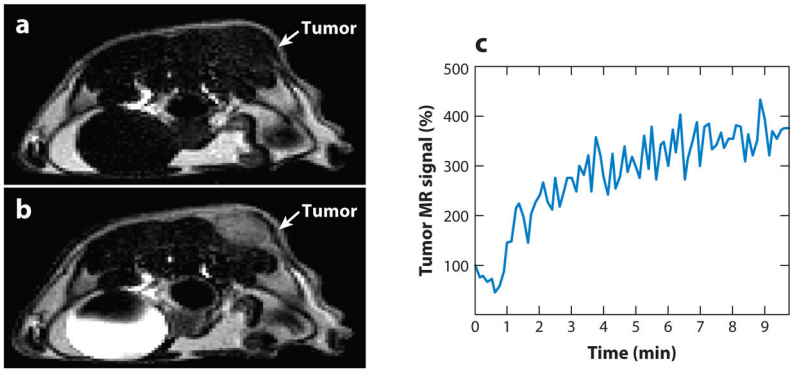

Figure 1.

Contrast enhancement of pathological tissues with a T_1 magnetic resonance imaging (MRI) contrast agent. (*a*) The tumor of an MDA-MB-231 mammary carcinoma model is difficult to identify without the MRI contrast agent. (*b*) T_1 contrast agent Gd-DTPA (Magnevist™) accumulated in the tumor and enhanced the image contrast for the tumor. (*c*) The temporal change in the T_1-weighted MR signal of the tumor confirmed that the contrast enhancement was due to accumulation of the agent. Reproduced with permission from Reference 9.

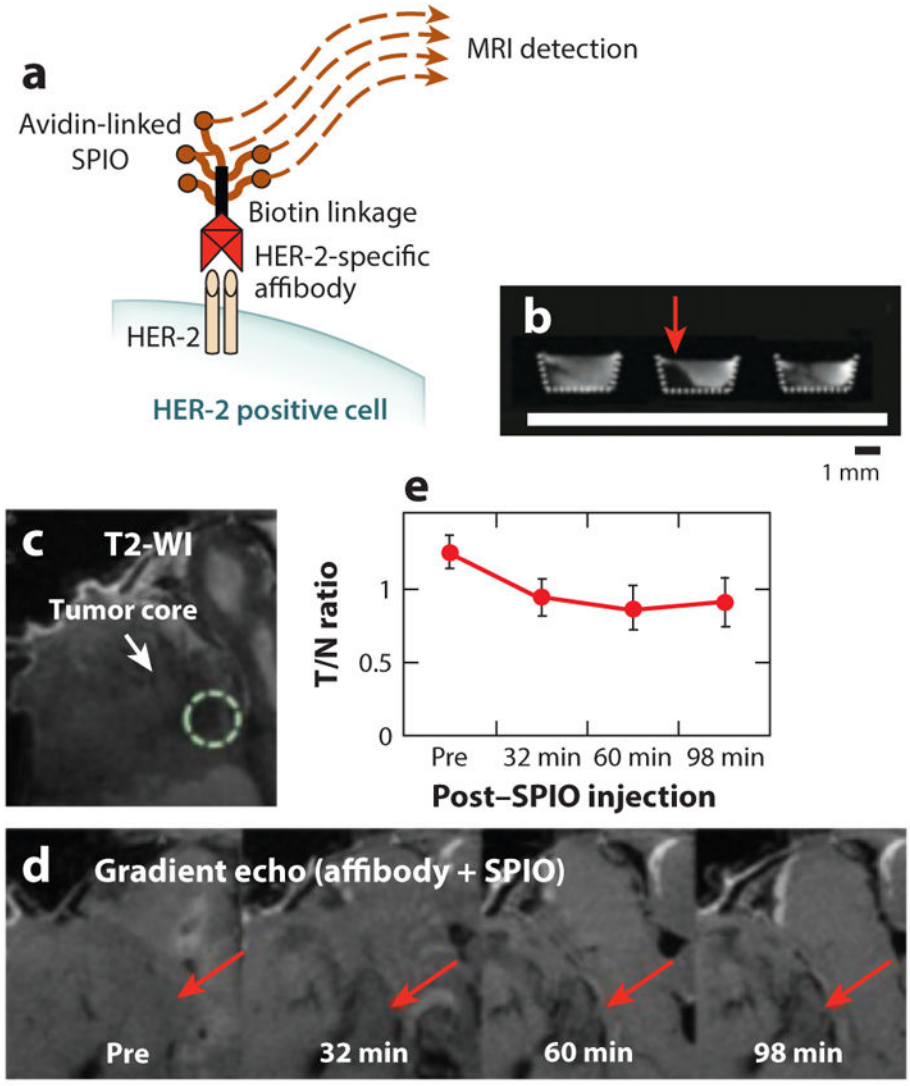

Figure 2.

Detecting cell receptors with T_2^* magnetic resonance imaging (MRI). (*a*) Schematic of an affibody-SPIO specific for HER-2. (*b*) An in vitro study detected HER-2-expressing human SKOV-3 ovarian cancer cells only when treated with the biotinylated affibody and avidin-linked SPIO (*red arrow*, *center*), but not after treatment only with avidin-linked SPIO (*left*), or if pretreated with a blocking antibody (*right*).

(*c*) T_2-weighted image showing the location of the tumor in a mouse model of SKOV-3 ovarian cancer. (*d*) T_2^*-weighted images before and after SPIO injection was performed 4 h after affibody administration. Red arrows indicate decreased image signal demonstrating HER-2 expression. (*e*) The ratio of the MRI signal of the tumor versus normal tissue quantified this temporally decreasing MR signal. Reproduced with permission from Reference 30.

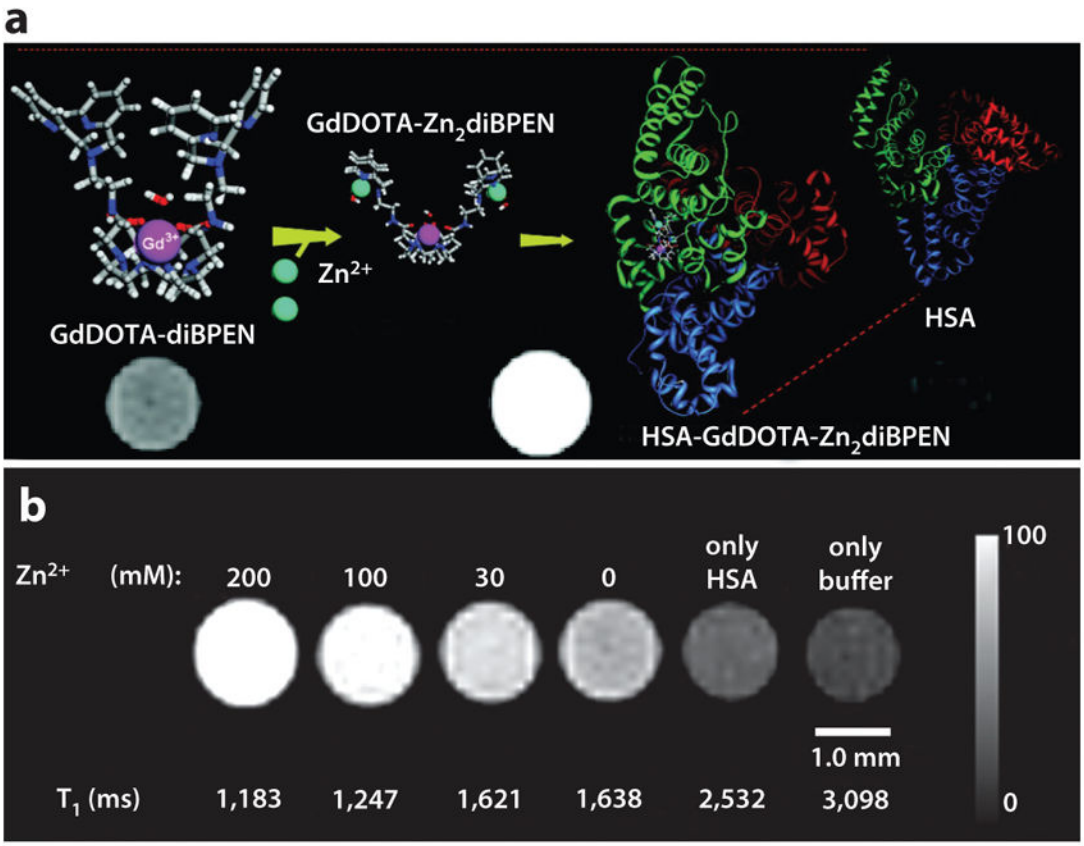

Figure 3.

Zinc detection with a T_1 magnetic resonance imaging (MRI) contrast agent. (*a*) The contrast agent GdDOTA-diBPEN can bind to Zn^{2+} and then tightly bind to human serum albumin (HSA), causing a T_1-weighted image to become brighter. (*b*) T_1-weighted MR images and T_1 relaxation times of samples containing 100 μM of the contrast agent with a physiologically relevant concentration of HSA and a range of Zn^{2+} concentrations show that 30 mM of Zn^{2+} can be detected with this contrast agent. Reproduced with permission from Reference 36.

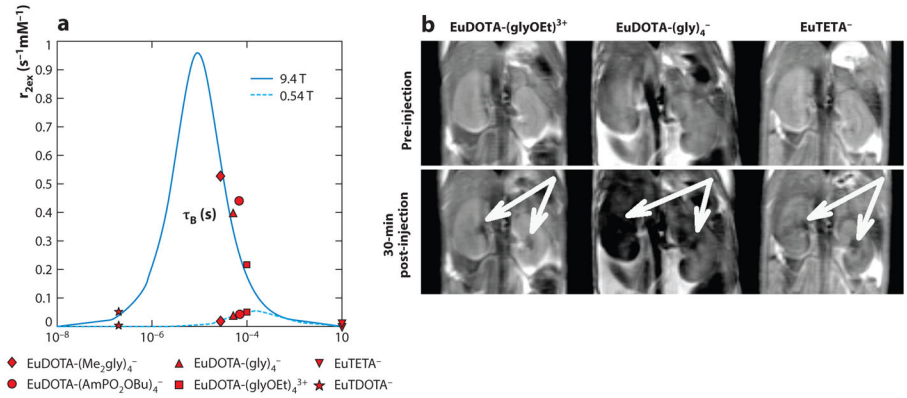

Figure 4.

T_{2ex} magnetic resonance imaging (MRI). (*a*) The r_{2ex} relaxivity plotted relative to the bound water lifetime for multiple Eu(III) chelates at 9.4-T magnetic field strength (*solid line*) shows that contrast agents with a moderately fast chemical exchange rate can generate a T_{2ex} effect. A lower T_{2ex} effect is generated at 0.54 T (*dotted line*). (*b*) Coronal images of mouse kidneys before and after IV injection of $EuDOTA^{-}$, EuDOTA-$(gly)_4^{-}$, and $EuTETA^{-}$ show that the T_{2ex} effect of EuDOTA-$(gly)_4^{-}$ in kidney tissues causes the image to become dark (*white arrows*). Reproduced with permission from Reference 40.

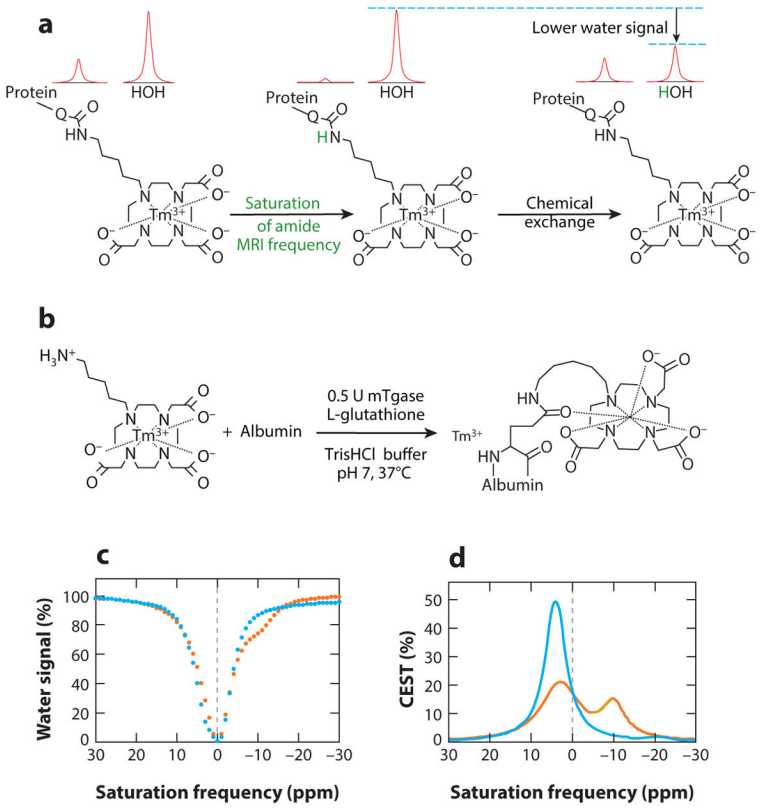

Figure 5.

Detection of enzyme activity with chemical exchange saturation transfer magnetic resonance imaging (CEST MRI). (*a*) The amide proton of the agent undergoes MR saturation (*green*) and is then transferred to water via chemical exchange, resulting in saturation of part of the water MR signal. (*b*) Transglutaminase can conjugate the agent to the glutamine side chain of a protein, which can generate a CEST signal. (*c*) CEST spectra and (*d*) a Lorentzian line-shape spectrum before (*orange*) and after (*blue*) TGase is incubated with the contrast agent. The appearance of a CEST effect at −9.2 ppm and the disappearance of CEST at +4.6 ppm indicate TGase catalysis of the bond formation. Reproduced with permission from Reference 66.

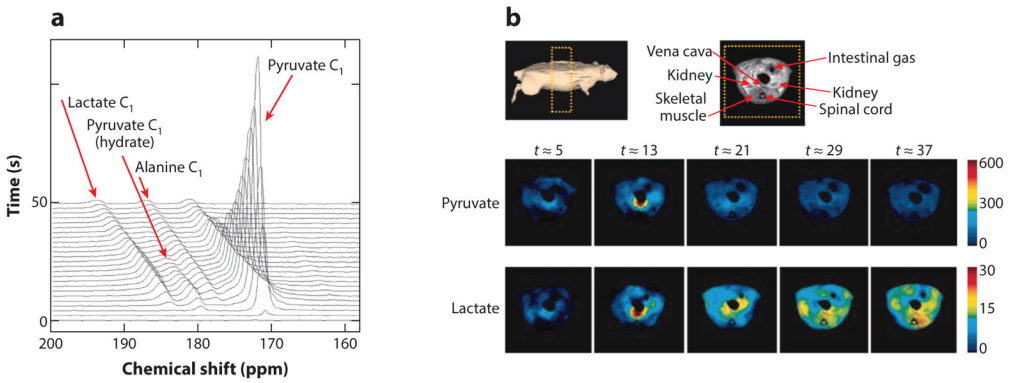

Figure 6.

In vivo detection of the conversion of pyruvate to lactate using hyperpolarized ^{13}C magnetic resonance imaging (MRI). (*a*) Stack of MR spectra showing the time course of the decay of pyruvate and the buildup of lactate in the MR image of a rat. (*b*) ^{1}H MR image of the rat showing the location of muscle. Temporal parametric maps of the biodistributions of pyruvate and lactate show the production of lactate in muscle. Reproduced with permission from Reference 98.